Molekul, Vol. 14. No. 2, November 2019: 140 – 148

MOLEKUL
www.jmolekul.com

Articles

https://doi.org/10.20884/1.jm.2019.14.2.570

Synthesis and Characterization of TiO_2-CaO and TiO_2-CaO-Fe_2O_3 Photocatalyst for Removal of Catechol

Candra Yulius Tahya[1*], Wahyu Irawati[2], Karnelasatri[1], Friska Juliana Purba[1]

[1]Study Program of Chemistry Education, Faculty of Education, Universitas Pelita Harapan, Tangerang, Indonesia
[2]Study Program of Biology Education, Faculty of Education, Universitas Pelita Harapan, Tangerang, Indonesia

*Corresponding author email: candra.tahya@uph.edu

Received August 29, 2019; **Accepted** October 31, 2019; **Available online** November 30, 2019

ABSTRACT. TiO_2-CaO and TiO_2-CaO-Fe_2O_3 photocatalysts have been synthesized through the surfactant-assisted sol-gel method. The catalysts were characterized using XRD, FTIR, SEM-EDS and BET surface area. XRD pattern showed the formation of anatase TiO_2 crystal phase both in TiO_2-CaO and TiO_2-CaO-Fe_2O_3. The TiO_2-CaO has higher crystallinity than TiO_2-CaO-Fe_2O_3. Based on the peak refinement using Rietveld, there are two peaks identified as Fe_2O_3 hematite in the sample TiO_2-CaO-Fe_2O_3. BET surface area analysis showed that the average pore size of TiO_2-CaO and TiO_2-CaO-Fe_2O_3 catalysts are 8.04 and 8.41 nm respectively, indicating both catalysts are mesoporous. FTIR spectra show that the vibration of Ti-O, Ca-O, and Ca-TiO_2 were observed in both catalysts. SEM images confirm that both catalysts are porous material. The catechol removal using TiO_2-CaO and TiO_2-CaO-Fe_2O_3 improved with the increase of catalyst concentration. After 360 minutes of UV radiation, the removal of catechol using TiO_2-CaO-Fe_2O_3 reached 46.0%, 48.3%, and 69.2%, while when using TiO_2-CaO, it reached 22.1%, 36.8%, and 57.0% for 0.1 g, 0.15 g, and 0.2 g of catalysts, respectively. The photocatalytic activity of TiO_2-CaO-Fe_2O_3 is not so strong compared to TiO_2-CaO catalyst but the catechol adsorption property of TiO_2-CaO-Fe_2O_3 is higher than that of TiO_2-CaO catalyst.

Keywords: Photocatalyst, Sol-gel, Removal of Catechol, TiO_2-CaO-Fe_2O_3

INTRODUCTION

Titanium oxide (TiO_2) is one of the most well-known materials for photocatalytic activity because TiO_2 has low cost, high oxidizing ability and chemical stability, non-toxic and safety for environment characteristics (Cao et al., 2000; Tseng, Lin, Chen, & Chu, 2010). TiO_2 has three polymorphic forms i.e. anatase, brookite, and rutile, but the anatase phase has been proved to be a higher activity of photocatalytic material (Phattepur, Siddaiah, & Ganganagappa, 2019). However, it is necessary to get enough light intensity that possesses the energy to overcome TiO_2 anatase band gap energy (3.2 eV) for photocatalytic reaction to proceed. In recent years, many transition metal ion-doped TiO_2 have been studied to improve the photocatalytic activity of such as Pt, Au, Pd, Ru and Fe (Tseng et al., 2010) and shows good results. While other researchers also have investigated the photocatalytic property of Ca doped-TiO_2 (Fatimah, Rahmadianti, & Pudiasari, 2018; Liu, Min, Hu, & Liu, 2014) and showed good ability to remove thiophene and methylene blue under light radiation. Besides TiO_2, there is some semiconductor that has been investigated as photocatalyst i.e. ZnO, GaP, SiC and Fe_2O_3 (R. Hoffmann, T. Martin, Choi, & W. Bahnemann, 2002). Moniz et al. have synthesized Fe_2O_3-TiO_2 nanocomposite and it shows remarkable enhancement in photocatalytic activity for removal of contaminant herbicide (Moniz, Shevlin, An, Guo, & Tang, 2014).

In this research, TiO_2-CaO and TiO_2-CaO-Fe_2O_3 catalysts were synthesized by surfactant-assisted Sol-gel method. It becomes interesting to investigate the influence of adding Fe_2O_3 into the structure of TiO_2-CaO. Composite Fe_2O_3 is well-known for its photocatalytic activity but it also has good affinity to phenol derivate compound (Malligavathy, Iyyapushpam, Nishanthi, & Padiyan, 2016), so by adding Fe_2O_3 into TiO_2-CaO structure, the removal of phenol derivate compound could be enhanced.

The catalyst is synthesized by sol-gel method. It can be implemented under the mild condition to produce material in various sizes, formats and shapes (Tseng et al., 2010). The sol-gel method has several advantages (Tseng et al., 2010) such as (1) inexpensive and easy to

be conducted, (2) lower temperature of preparation, (3) better purity from raw material, (4) better mixing for a system of multi-component, etc. The use of surfactants to assist the synthesis of catalysts via the sol-gel method has been widely carried out (Anderson & Binions, 2014; Galkina, Vinogradov, Agafonov, & Vinogradov, 2011; Phattepur et al., 2019; Torres-Romero, Cajero-Juárez, & Contreras-García, 2017), and the use of tween surfactant has been proven to increase photocatalyst activity and absorption of harmful organic substances (Anderson & Binions, 2014).

Phenol derivate compounds have many benefits for industrials like textile, chemical and petrochemical, pharmaceutical, mining, and pulp (Malligavathy et al., 2016). Catechol is one of the phenol derivate compounds. Around 20 thousand tons of catechol annually are synthetically produced for organic chemical commodities such as flavorings, fragrances (vanillin), pharmaceuticals, and especially (around 50%) are used as precursors of pesticides (Fiege et al., 2000). Because of the very large use of catechol, the level of catechol pollution to the environment also increases (Canadian Ministers of the Environment and of Health, 2008). To reduce the impact of pollution by catechol, it is necessary to research the degradation of hazardous pollutant chemicals. In this research, the process of degradation of catechol has been investigated through the mechanism of photodegradation and adsorption.

EXPERIMENTAL SECTION

Materials

Titanium (IV) butoxide ($Ti(OC_4H_{10})_4$), calcium oxide (CaO), hydrochloric acid (HCl), iron (III) chloride anhydrous ($FeCl_3$), tween 80, ethanol, catechol ($C_6H_4(OH)_2$), 4-aminoantipyrene, potassium ferricyanide ($K_3Fe(CN)_6$), ammonia (NH_3), and ammonium chloride (NH_4Cl) were purchased from Merck. Distilled water was used throughout experimental procedures. All Glass tools were purchased from Iwaki. Micropipette miniPCR was used for measuring of the sample in µL scale.

Synthesis of Materials

TiO_2-CaO-Fe_2O_3 photocatalyst was synthesized by surfactant-assisted sol-gel method using a precursor of Titanium (IV) butoxide with molar ratio of Ti : Ca : Fe is 7 : 1 : 1. Prepare solution 1 dan solution 2 as follows. Solution 1 was composed of 4 mL of ethanol mixed with 2 mmol CaO. Solution 2 was composed of 8 mL of ethanol mixed with 4 mL titanium (IV) butoxide, 2 mmol $FeCl_3$, tween 80 0.5 mL and 0.3 mL concentrated hydrochloric acid.

Solution 1 and 2 were mixed and stir vigorously for 30 min until the gel formed. Then the gel was dried at 90 °C for 12 hours in a hot air oven. The dried solid was ground and subjected to calcination from 27 °C to 500 °C with heating rate 5 °C per 30 seconds and maintain at 500 °C for 3 hours. The catalyst TiO_2-CaO-Fe_2O_3 was cooled until reached room temperature for 1 night. The TiO_2-CaO photocatalyst was synthesized with the same procedure but without $FeCl_3$. The molar ratio of Ti : Ca is 7 : 1 (Liu et al., 2014).

Characterization of materials

The structural characterization of TiO_2-CaO-Fe_2O_3 and TiO_2-CaO photocatalysts were carried out using X-ray diffractometer (XRD) Empyrean with refinement using Rietveld analysis (Lutterotti & Scardi, 1990), scanning electron microscopy-energy dispersive spectroscopy (SEM-EDS) to see the particle size and the atomic composition, Fourier transform infra-red (FTIR) to see the atomic bonding vibration of catalysts, and Brunauer – Emmet – Teller (BET) surface area analyzer.

Photocatalyst Reactor Set Up

The simple photocatalyst reactor was set up as showed in **Figure 1.** It consists of three UV lamp (total 49 W, wavelength 254 nm), a multi-position magnetic stirrer. The walls of the reactor container are coated with aluminum foil to minimize the absorption of UV light on the walls of the container. A sample solution containing 100 mL of 100 mg/L catechol was filled into an Erlenmeyer flask capacity of 100 mL. The magnetic bar has also been placed in the flask for stirring at 100 rpm when the UV lamp was turned on.

The walls of the reactor container are coated with aluminum foil to minimize the absorption of UV light on the walls of the container. A sample solution containing 100 mL of 100 mg/L catechol was filled into an Erlenmeyer flask capacity of 100 mL. The magnetic bar has also been placed in the flask for stirring at 100 rpm when the UV lamp was turned on.

Catechol Photodegradation

Catechol photodegradation was carried out by preparing 100 mL of 100 mg/L catechol solution into Erlenmeyer flask with a capacity of 100 mL and adding a variety of weight the TiO_2-CaO-Fe_2O_3 and TiO_2-CaO catalysts. The mixture was stirred for 60 minutes in dark conditions aimed at achieving a steady state, then the UV light is turned on. The system is maintained, and every 60 minutes, about 5 mL samples are taken, then filtered using a microfilter nylon syringe with a pore diameter of 0.45 nm. A total of 500 µL of sample filtrate was taken and added with 7000 µL of distilled water, 2000 µL of ammonia buffer, 300 µL of 2% aminoantipyrine solution and 200 µL of 8% $K_3Fe(CN)_6$ solution and stirred evenly. Leave the mixture for 15 minutes at room temperature to react and form pink color. The absorbance of this dye was measured using a spectrophotometer BK-UV 1000 Biobase at a

wavelength of 460 nm (Liŭ, Li, Wang, Wang, & Liú, 2016). Blank is a sample of catechol solution replaced with 500 µL distilled water. Calculation of the catechol photodegradation efficiency which is similar to catechol removal efficiency is carried out using equation 1:

$PE = (A_o - A_t)/A_o \times 100$ ..... (1)

Where A_o = absorbance at time zero hours.

A_t = absorbance at time t hours.

RESULTS AND DISCUSSION

X-ray diffraction patterns and refinement with Rietveld.

XRD patterns peak at 2θ = 25.53°, 37.33°, 48.27°, 54.24°, 55.36°, and 62.86° confirm the TiO_2 anatase phase in TiO_2-CaO, and peak at 2θ = 25.43°, 37.43°, 48.34°, 54.19°, 55.03°, and 62.70° confirm the TiO_2 anatase phase in TiO_2-CaO-Fe_2O_3 catalysts.

The refinement of XRD shows sample TiO_2-CaO-Fe_2O_3 contains 91.78% weight percentage of TiO_2 anatase and 8.22% weight percentage of Fe_2O_3 hematite. The hematite phase was exhibited by peaks at 2θ = 33.25° and 35.72°. X-ray diffraction pattern showed the formation of anatase TiO_2 crystal phase in both catalysts. The TiO_2-CaO showed higher crystallinity than TiO_2-CaO -Fe_2O_3. According to Malliga vathy et al. the increased crystallite size could cause the decrease of the band gap, and it has a direct relation to the increase of removal efficiency (Malligavathy et al., 2016). Therefore, decreasing crystallite size in TiO_2-CaO-Fe_2O_3 could probably cause a decreasing of photocatalytic efficiency.

Catalyst TiO_2-CaO contains single-phase TiO_2 anatase with the crystal structure parameters listed in **Table 1**. Catalyst TiO_2-CaO-Fe_2O_3 contains (i) TiO_2 anatase and (ii) Fe_2O_3 hematite with the crystal structure parameters listed in **Table 2**.

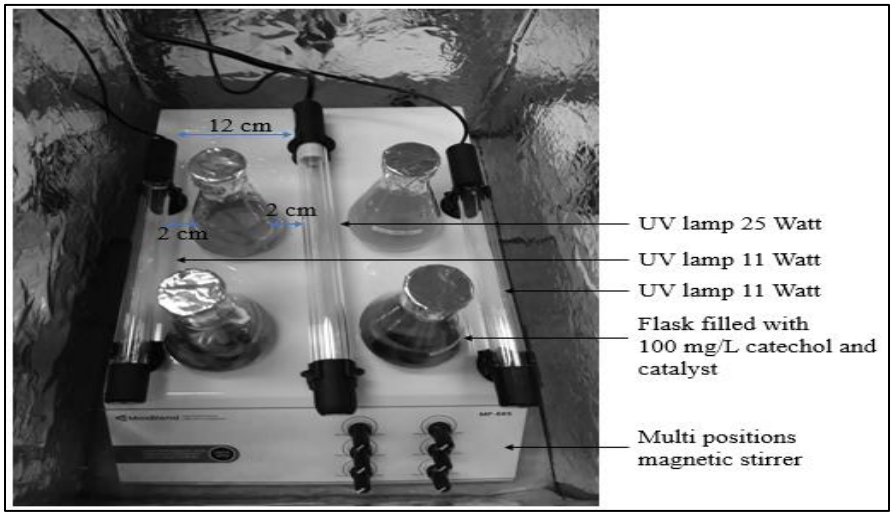

Figure 1. The simple photocatalyst reactor.

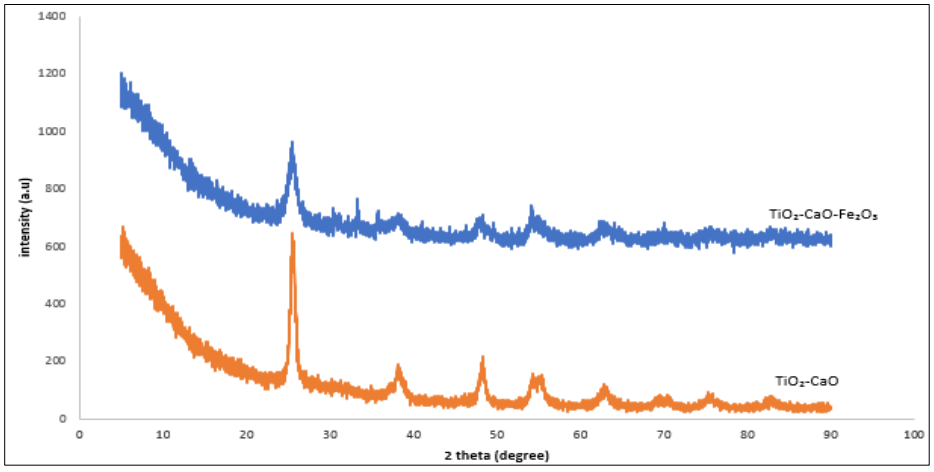

Figure 2. The XRD pattern of TiO_2-CaO and TiO_2-CaO-Fe_2O_3

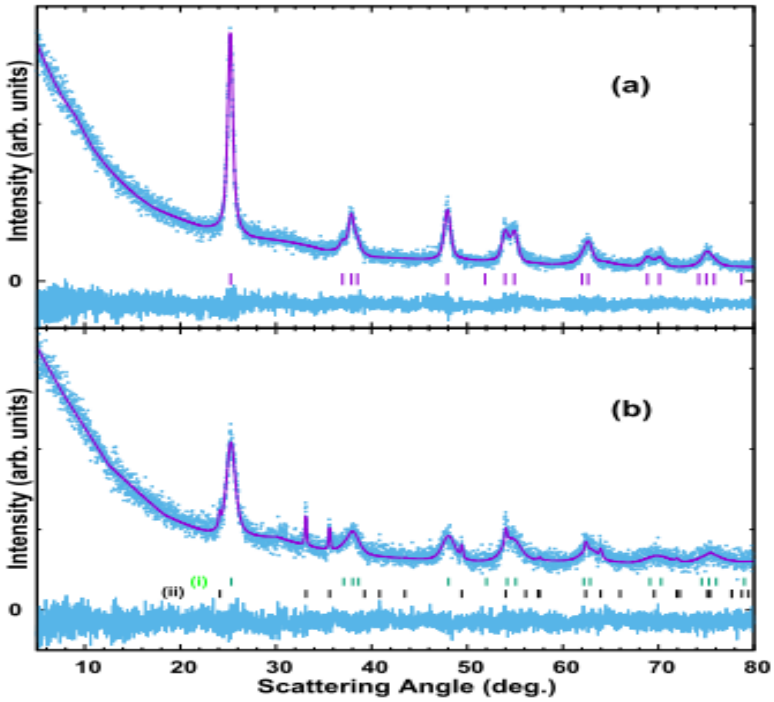

Figure 3. Rietveld Refinement profiles of (a) TiO_2-CaO and (b) TiO_2-CaO-Fe_2O_3.

Table 1. Lattice parameters of TiO_2-CaO

Chemical Name:	TiO_2, Anatase
Crystal system:	Tetragonal
Space group:	$I4_1/amd$
Density (g/cc):	3.92
Lattice Parameters:	a = b(Å): 3.771 c(Å): 9.43

Table 2. The lattice parameter of TiO_2-CaO-Fe_2O_3

Chemical Name:	TiO_2, Anatase	Fe_2O_3, Hematite
Crystal system:	Tetragonal	Trigonal
Space group:	$I4_1/amd$	R -3 c:R
Density (g/cc):	3.92	5.26
Lattice Parameters:	a = b(Å): 3.771 c(Å): 9.43	a = b = c(Å): 5.43 α = β = γ(°): 55.28

Scanning Electron Microscopy-Energy Dispersive Spectroscopy (SEM-EDS)

The SEM-EDS results of TiO_2-CaO catalyst are shown in **Figure 4**. SEM image indicates the morphology of TiO_2-CaO as a porous material, but the particle size is larger than 5 µm. The EDS analysis shows the mass ratio of Ti:Ca:O is 43.6 : 3.6 : 46.3. The SEM-EDS results of TiO_2-CaO-Fe_2O_3 catalyst are shown in **Figure 5**. SEM image indicates the morphology of TiO_2-CaO-Fe_2O_3 also as a porous material, but the particle size is larger than 5 µm. The EDS analysis shows the mass ratio of Ti:Ca:O:Fe is 36.9 : 8.5 : 43.1 : 3.6.

The SEM images show that there is a difference between the surface structure of TiO_2-CaO and TiO_2-CaO-Fe_2O_3 catalyst. It could be observed many holes in the surface of TiO_2-CaO catalyst. These holes are caused by the removal of an organic molecule such as ethanol and tween 80 during the calcination process. The hole surface structure is not observed in TiO_2-CaO-Fe_2O_3 catalyst because of the presence of Fe^{3+} in solution. Fe^{3+} ion interacts with surfactant tween 80 as a chelating agent (Kyzas, Peleka, & Deliyanni, 2013; Suah, Faiz Bukhari Mohd, Musa Ahmad, 2017) and could slow down the oxidation rate during calcination so the hole surface does not form.

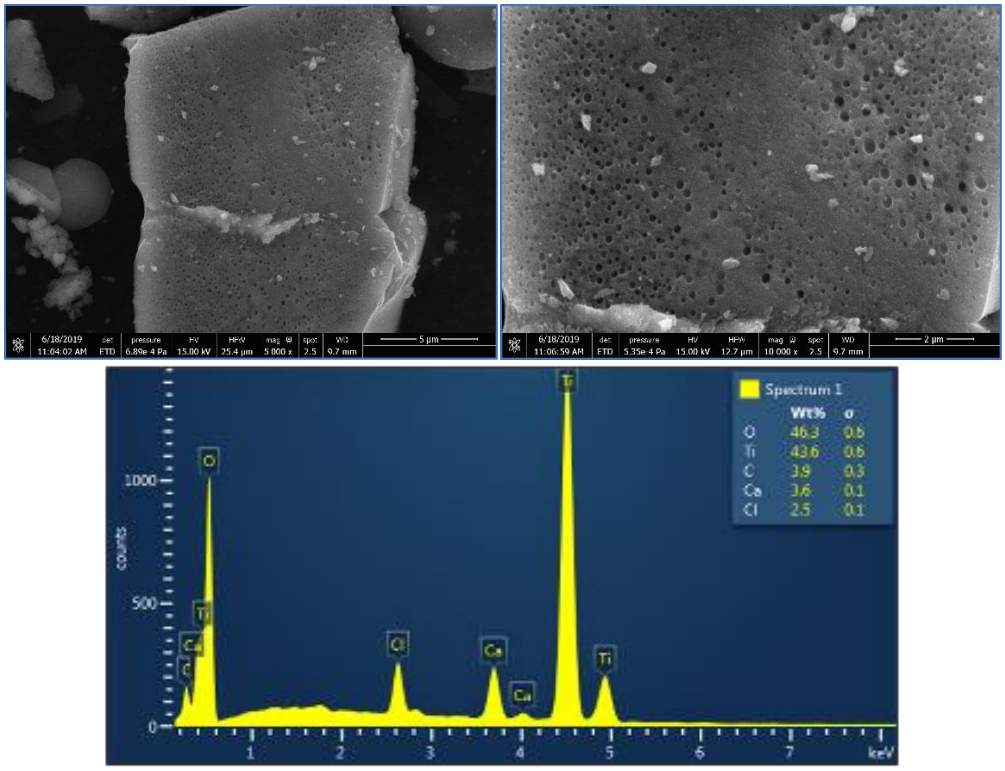

Figure 4. SEM and EDS results of TiO_2-CaO catalyst

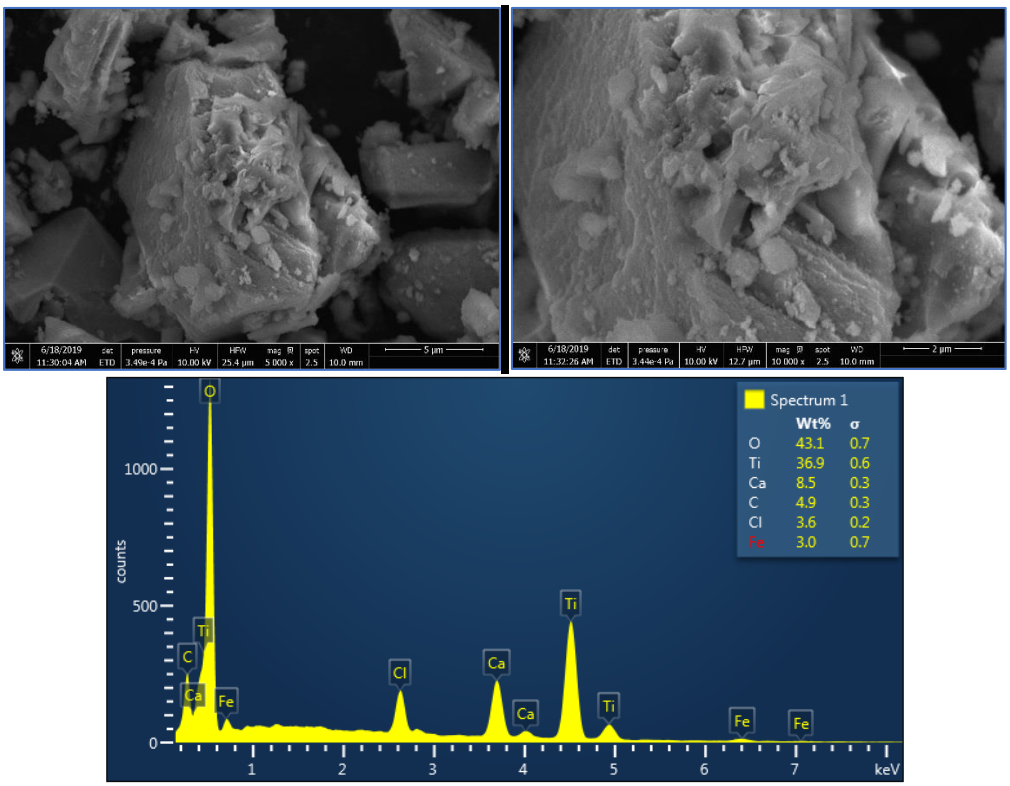

Figure 5. SEM and EDS results of TiO_2-CaO-Fe_2O_3 catalyst

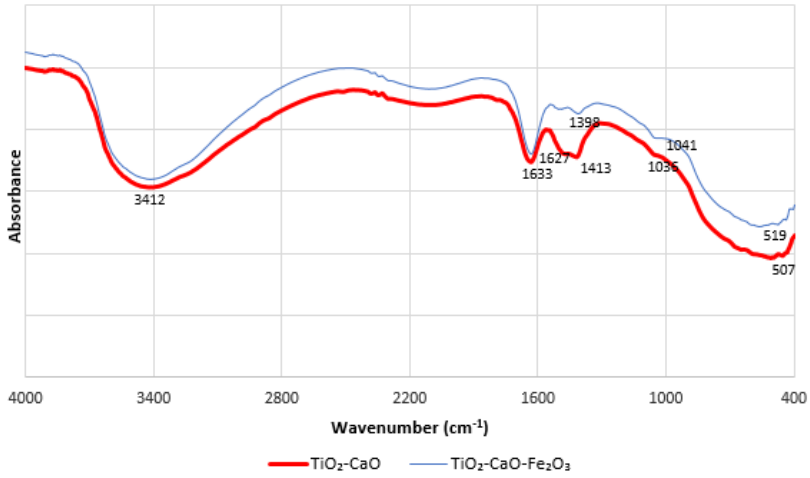

Figure 6. FTIR spectra of TiO_2-CaO and TiO_2-CaO-Fe_2O_3 catalysts

Table 3. BET Surface area result of TiO_2-CaO and TiO_2-CaO-Fe_2O_3 catalysts

Sample	BET specific surface area, m^2/g	Average pore size, nm	Pore volume, cm^2/g	Average particle size, nm
TiO_2-CaO	84.78 ± 1.360	8.04290	0.170	70.7746
TiO_2-CaO-Fe_2O_3	60.63 ± 0.879	8.41036	0.127	98.9625

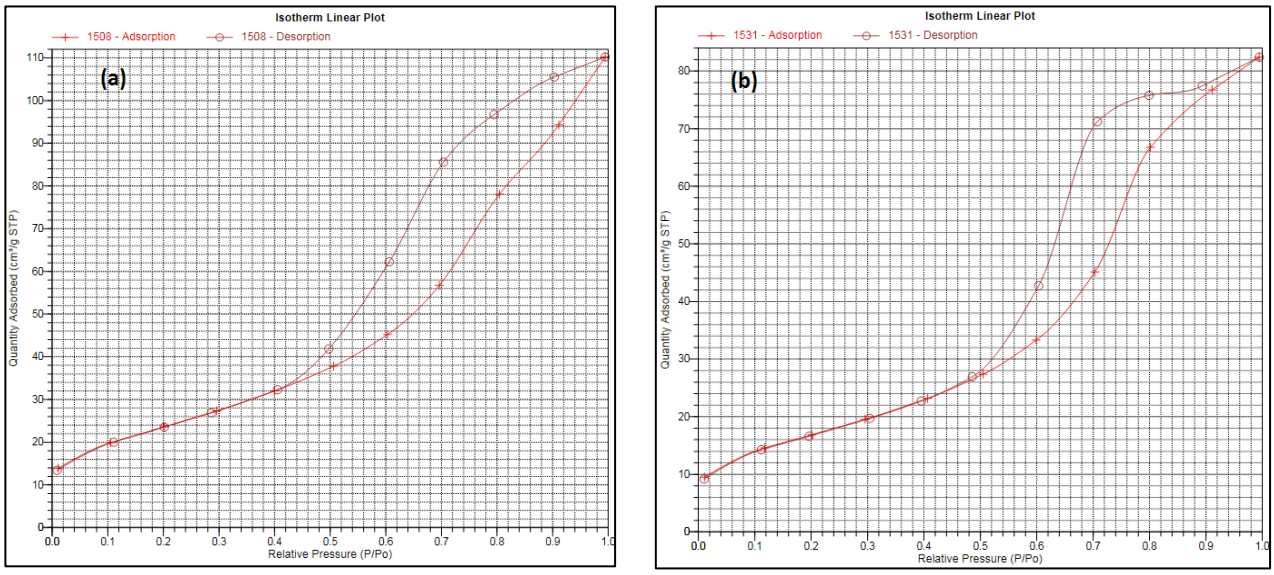

Figure 7. Nitrogen (N_2) physisorption isotherms of (**a**) TiO_2-CaO and (**b**) TiO_2-CaO-Fe_2O_3 catalysts

Fourier Transform Infrared Spectroscopy

The FTIR spectra of TiO_2-CaO-Fe_2O_3 catalysts show several important peaks. The wavenumber of 519 cm^{-1} corresponds to the stretching vibration of Ti-O-Ti bonding. The wavenumber of 1041 cm^{-1} corresponds to the vibration of Ca-O bond (low peak because of the low content of CaO (Liu et al., 2014)). The wavenumber of 1398 cm^{-1} corresponds to the vibration of Ca-TiO_2 which is absent for pure TiO_2 (Liu et al., 2014). The wavenumber of 1627 cm^{-1} and 3412 cm^{-1} correspond to the O-H vibration of surface-absorbed water. The stretching vibration of Fe-O bonding would be present in 573 – 579 cm^{-1} (Benjwal, Kumar, Chamoli, & Kar, 2015; Zhang et al., 2017). Fe-O vibration band is not

clear observed because it coincides with the Ti-O vibration in wave number below 600 cm^{-1}.

The FTIR spectra of TiO_2-CaO catalysts show several important peaks. The wavenumber of 507 cm^{-1} corresponds to the stretching vibration of Ti-O-Ti bonding. The wavenumber of 1036 cm^{-1} also appears which corresponds to vibration of Ca-O bond. The wavenumber of 1412 cm^{-1} corresponds to vibration of Ca-TiO_2. The wavenumber of 1627 cm^{-1} and 3412 cm^{-1} correspond to the O-H vibration of surface-absorbed water.

BET Surface Area Analysis

The average pore size of TiO_2-CaO and TiO_2-CaO-Fe_2O_3 were 8.04 and 8.41 nm respectively, indicate that both catalysts were mesoporous. The mesoporous TiO_2/Fe_2O_3 photocatalysts were also reported by Palanisamy et al. which was synthesized through sol-gel methods (Palanisamy, Babu, Sundaravel, Anandan, & Murugesan, 2013). Nitrogen (N_2) physisorption isotherms of both catalysts shown in **Figure 7**. Both catalysts show the adsorption-desorption isotherm as type IVa with H2(b)-type hysteresis loop (Thommes et al., 2015). TiO_2-CaO has a higher specific surface area (84.78 ± 1.360 m^2/g) than TiO_2-CaO-Fe_2O_3 (60.63 ± 0.879 m^2/g).

Photocatalytic Activity of TiO_2-CaO and TiO_2-CaO-Fe_2O_3 for Removal of Catechol

The photocatalytic activity of TiO_2-CaO and TiO_2-CaO-Fe_2O_3 were evaluated by degradation of 100 mg/L catechol solution in natural pH and the result was shown in **Figure 8**. The photocatalytic efficiency of TiO_2-CaO and TiO_2-CaO-Fe_2O_3 is improved with the increasing of catalyst concentration. After 360 minutes of UV radiation, the removal of catechol by using TiO_2-CaO-Fe_2O_3 reached 46.0%, 48.3%, and 69.2% for 0.1 g, 0.15 g, and 0.2 g of catalysts respectively. Meanwhile, for TiO_2-CaO, the removal of catechol reached 22.1%, 36.8%, and 57.0% for 0.1 g, 0.15 g, and 0.2 g of catalysts respectively. Catechol solution without catalyst was used as control. The removal of catechol without a catalyst is less than 2%. **Figure 8** showed the adsorptions of catechol by the surface of catalysts in dark condition. To investigate the catechol adsorption property of TiO_2-CaO and TiO_2-CaO-Fe_2O_3, the catechol removal in dark condition and in light was calculated. The results are shown in **Figure 9**.

Based on **Figure 9**, the photocatalytic activity of TiO_2-CaO-Fe_2O_3 is not so strong compared to TiO_2-CaO catalyst. Without UV radiation, TiO_2-CaO-Fe_2O_3 could remove the catechol until 62.8% after 360 minutes of reaction. Whereas under UV radiation, the catechol removal is 69.2%. The photocatalytic activity of TiO_2-CaO-Fe_2O_3 improves after 360 minutes whereas the TiO_2-CaO showed that the photocatalytic activity was observed from the first 120 minutes. However, the catechol adsorption property of TiO_2-CaO-Fe_2O_3 is higher than that of TiO_2-CaO catalyst. The intercalation of Fe_2O_3 in the structure of TiO_2-CaO catalyst has been created which decreases the crystallite size of TiO_2-CaO-Fe_2O_3 (as observed in XRD result). Because the Fe_2O_3 has a strong affinity toward catechol, the removal of catechol from solution is higher than in TiO_2-CaO catalyst.

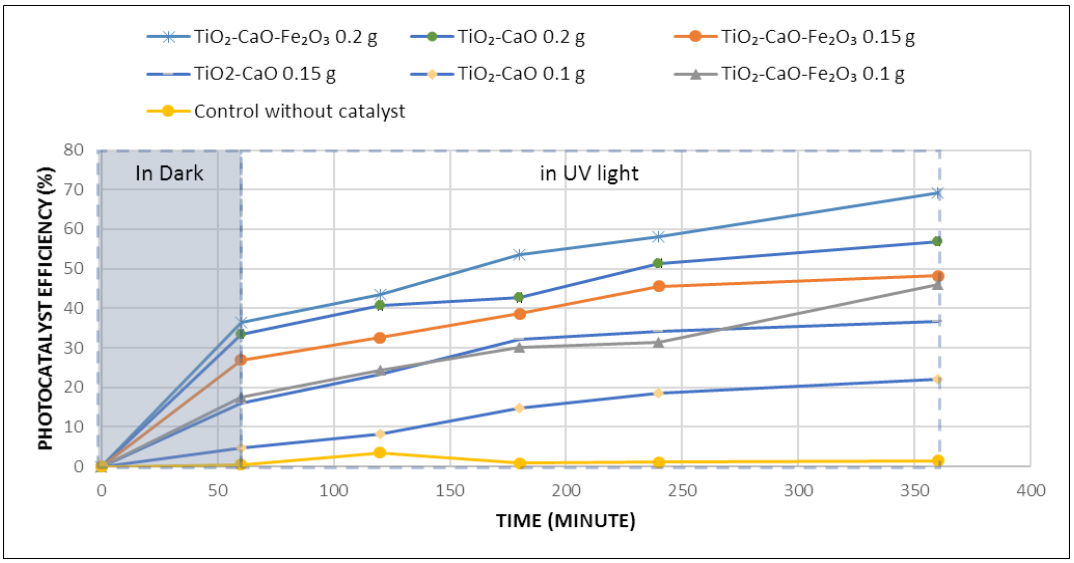

Figure 8. Effect of TiO_2-CaO and TiO_2-CaO-Fe_2O_3 on photocatalytic degradation of catechol at natural pH. Catechol concentration is 100 mg/L. Dosage: 0.1 g, 0.15 g, and 0.2 g per 100 mL solution for each catalyst.

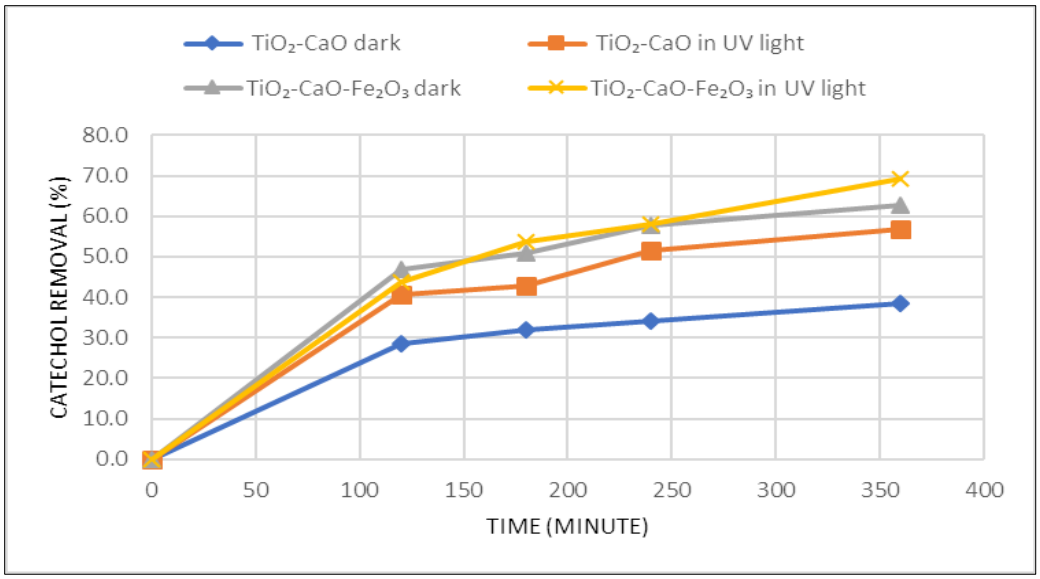

Figure 9. Effect of TiO_2-CaO and TiO_2-CaO-Fe_2O_3 on catechol removal at natural pH in dark condition compared to light condition. Dosage: 0.2 g catalyst per 100 mL solution.

CONCLUSIONS

The photocatalysts of TiO_2-CaO and TiO_2-CaO-Fe_2O_3 have been successfully synthesized through the sol-gel method. XRD pattern showed the formation of anatase TiO_2 crystal phase both in TiO_2-CaO and TiO_2-CaO-Fe_2O_3. FTIR spectra show that the vibration of Ti-O and Ca-O were observed in both catalysts. The average pore size of TiO_2-CaO and TiO_2-CaO-Fe_2O_3 catalysts are 8.04 and 8.41 nm respectively, indicating both catalysts are mesoporous. These catalysts exhibit photocatalytic and adsorption activities for removal of catechol. The TiO_2-CaO-Fe_2O_3 could remove the catechol until 62.8% and 69.2% after 360 minutes of reaction in dark and UV radiation, respectively. Meanwhile, TiO_2-CaO could remove the catechol until 38.6% and 57.0% after 360 minutes of reaction in dark and under UV radiation, respectively.

ACKNOWLEDGEMENTS

Thanks to Universitas Pelita Harapan, for financial support of this work. The research number provided by Center for Research and Community Service UPH is P-044-FIP/I/2019.

REFERENCES

Anderson, A. L., & Binions, R. (2014). The effect of Tween® Surfactants in sol-gel processing for the production of TiO_2 thin films. *Coatings*, *4*(4), 796–809.

Benjwal, P., Kumar, M., Chamoli, P., & Kar, K. K. (2015). Enhanced photocatalytic degradation of methylene blue and adsorption of arsenic(iii) by reduced graphene oxide (rGO)-metal oxide (TiO_2/Fe_3O_4) based nanocomposites. *RSC Advances*, *5*(89), 73249–73260.

Canadian Ministers of the Environment and of Health. (2008). 1,2-Benzenediol (Catechol), 1–25.

Cao, L., Gao, Z., Suib, S. L., Obee, T. N., Hay, S. O., & Freihaut, J. D. (2000). Photocatalytic oxidation of toluene on nanoscale TiO_2 catalysts: studies of deactivation and regeneration. *Journal of Catalysis*, *196*(2), 253–261.

Fatimah, I., Rahmadianti, Y., & Pudiasari, R. A. (2018). Photocatalyst of perovskite $CaTiO_3$ nanopowder synthesized from CaO derived from snail shell in comparison with the use of CaO and $CaCO_3$. *IOP Conference Series: Materials Science and Engineering*, *349*(1).

Fiege, H., Voges, H.-W., Hamamoto, T., Umemura, S., Iwata, T., Miki, H., Fujita, Y., Buysch, H.-J., Garbe, D., & Paulus, W. (2000). Phenol Derivatives. In *Ullmann's Encyclopedia of Industrial Chemistry*. American Cancer Society.

Galkina, O. L., Vinogradov, V. V., Agafonov, A. V., & Vinogradov, A. V. (2011). Surfactant-assisted sol-gel synthesis of TiO2 with uniform particle size distribution. *International Journal of Inorganic Chemistry*, *2011*, 1–8.

Kyzas, G. Z., Peleka, E. N., & Deliyanni, E. A. (2013). Nanocrystalline akaganeite as adsorbent for surfactant removal from aqueous solutions. *Materials*, *6*(1), 184–197.

Liŭ, D., Li, Z., Wang, W., Wang, G., & Liú, D. (2016). Hematite doped magnetic TiO_2 nanocomposites

with improved photocatalytic activity. *Journal of Alloys and Compounds*, *654*, 491–497.

Liu, S., Min, Z., Hu, D., & Liu, Y. (2014). Synthesis of calcium doped TiO_2 nanomaterials and their visible light degradation property, *2*(3), 2–6.

Lutterotti, L., & Scardi, P. (1990). Simultaneous structure and size-strain refinement by the rietveld method. *Journal of Applied Crystallography*, *23*(4), 246–252.

Malligavathy, M., Iyyapushpam, S., Nishanthi, S. T., & Padiyan, D. P. (2016). Optimising the crystallinity of anatase TiO_2 nanospheres for the degradation of Congo red dye. *Journal of Experimental Nanoscience*, *11*(13), 1074–1086.

Moniz, S. J. A., Shevlin, S. A., An, X., Guo, Z.-X., & Tang, J. (2014). Fe_2O_3–TiO_2 nanocomposites for enhanced charge separation and photocatalytic activity. *Chemistry – A European Journal*, *20*(47), 15571–15579.

Palanisamy, B., Babu, C. M., Sundaravel, B., Anandan, S., & Murugesan, V. (2013). Sol–gel synthesis of mesoporous mixed Fe2O3/TiO2 photocatalyst: Application for degradation of 4-chlorophenol. *Journal of Hazardous Materials*, *252–253*, 233–242.

Phattepur, H., Siddaiah, G. B., & Ganganagappa, N. (2019). Synthesis and characterisation of mesoporous TiO_2 nanoparticles by novel surfactant assisted sol-gel method for the degradation of organic compounds. *Periodica Polytechnica Chemical Engineering*, *63*(1), 85–95.

R. Hoffmann, M., T. Martin, S., Choi, W., & W. Bahnemann, D. (2002). Environmental Applications of Semiconductor Photocatalysis. *Chemical Reviews*, *95*(1), 69–96.

Suah, Faiz Bukhari Mohd, Musa Ahmad, F. S. M. (2017). Effect of non-ionic surfactants to the Al(III)-morin complex and its application in determination of Al(III) ions: A preliminary study. *Malaysian Journal of Analytical Science*, *21*(4), 793–800.

Thommes, M., Kaneko, K., Neimark, A. V., Olivier, J. P., Rodriguez-Reinoso, F., Rouquerol, J., & Sing, K. S. W. (2015). Physisorption of gases, with special reference to the evaluation of surface area and pore size distribution (IUPAC Technical Report). *Pure and Applied Chemistry*, *87*(9–10), 1051–1069.

Torres-Romero, A., Cajero-Juárez, M., & Contreras-García, M. E. (2017). Titania-ceria surfactant assisted sol-gel synthesis and characterization. *Epitoanyag - Journal of Silicate Based and Composite Materials*, *69*(1), 8–11.

Tseng, T. K., Lin, Y. S., Chen, Y. J., & Chu, H. (2010). A review of photocatalysts prepared by sol-gel method for VOCs removal. *International Journal of Molecular Sciences*, *11*(6), 2336–2361.

Zhang, T., Zhao, N., Li, J., Gong, H., An, T., Zhao, F., & Ma, H. (2017). Thermal behavior of nitrocellulose-based superthermites: Effects of nano-Fe_2O_3 with three morphologies. *RSC Advances*, *7*(38), 23583–23590.